

Laser-induced structure formation on stretched polymer foils

Nikita Biturin,^{1,*} Enno Arenholz,² Nikita Arnold,¹ and Dieter Bäuerle^{1,†}

¹Angewandte Physik, Johannes-Kepler-Universität, Altenbergerstraße 69, A-4040, Linz, Austria

²Voest Alpine AG, 4020 Linz, Austria

(Received 4 October 2006; revised manuscript received 7 February 2007; published 12 April 2007)

Noncoherent structures that develop during UV laser ablation of stretched semicrystalline polymer foils are a very general phenomenon. A thermodynamic model based on stress relaxation within the modified layer of the polymer surface describes the main features of the observed phenomena, and, in particular, the dependence of the period of structures on laser wavelength, fluence, and number of laser pulses.

DOI: 10.1103/PhysRevE.75.041603

PACS number(s): 82.65.+r, 82.50.Hp, 42.62.-b, 81.15.Fg

I. INTRODUCTION

Coherent- and noncoherent-structure formation on laser-irradiated surfaces in reactive and nonreactive ambient media has been discussed in Ref. [1]. Among the various different types of noncoherent structures are wall- and nap-type structures that develop on stretched polymer foils and fibers during laser ablation [1–7]. The occurrence of such structures is a very general phenomenon that has been observed with many different polymers such as polyimide (PI), polyethylene-terephthalate (PET), polyamide (PA), polyethylene-naphthalate (PEN), and others. The most detailed experimental investigations have been performed with PI and PET. The formation of wall- and nap-type structures has been attributed to the different optical and thermal properties of amorphous and crystalline regions within these polymers entailing differences in ablation rate [8], to hydrodynamic instabilities [2,3], and to nonuniform laser-induced defect formation within the polymer surface [9]. However, detailed investigations have clearly demonstrated that the formation of such structures is closely related to internal stresses within the foils or fibers [1,4–7]. Uniaxial stretching prior to laser-light irradiation results in wall-type structures with one-dimensional periodicity, while biaxial stretching gives rise to nap-type structures (two-dimensional periodicity). No structure formation of this type has been observed on foils that have been annealed (stress released) prior to laser-light irradiation. A simple model that considers the changes in elastic and surface energies due to stress relaxation has been discussed in Ref. [1].

In this paper we present a thermodynamic model that is based on the laser-induced relaxation of frozen-in stresses within the material surface. The model describes the main features observed during UV laser ablation of different types of polymer foils. In particular, it permits a semiquantitative interpretation of the dependence of the period of structures on laser wavelength, fluence, and the number of laser pulses.

II. EXPERIMENTAL OBSERVATIONS

Scanning electron microscope (SEM) pictures of wall- and nap-type structures observed on PET foils after

248 nm KrF laser ablation are shown in Fig. 1 (adapted from Ref. [7]). Similar pictures observed on PI foils are presented in Refs. [1,6]. Some of the most characteristic dependences of the period of such structures on laser parameters are summarized in Fig. 2 for the example of biaxially stretched PET foils (Dupont Mylar™, thickness 50 μm). With all wavelengths investigated, i.e., with 193 nm ArF-, 248 nm KrF-, and 308 nm XeCl-excimer laser radiation, the laser fluences employed were above the respective threshold fluences for ablation (see Table I). The figure clearly shows that the period of nap-type structures, Λ , increases with both the laser wavelength (optical penetration depth) and the number of laser pulses. Depending on these parameters and the laser fluence, Λ is within the range of about 0.5–50 μm. No influence of the laser pulse repetition rate on Λ was observed within the range 1–50 Hz. The dependence of the period Λ on the number of laser pulses N_ℓ remains unchanged for nanosecond (28 ns) and subpicosecond (500 fs) KrF-laser pulses. This is shown in Fig. 3. The increase in Λ with N_ℓ becomes less pronounced with an increasing angle of laser beam incidence [1]. Such a behavior is also observed with partially annealed foils with incomplete relaxation of frozen-in stresses [4]. No wall- and nap-type structures were

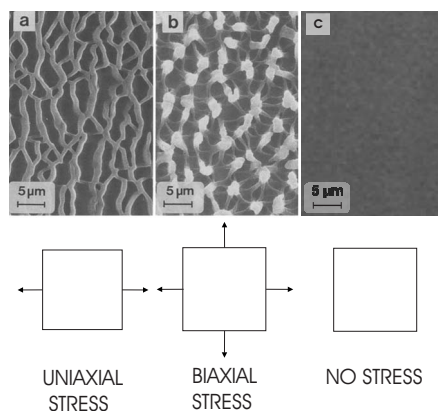


FIG. 1. SEM micrographs of different PET foils (Dupont Mylar™, thickness 50 μm) after ablation with 248 nm KrF laser radiation. (a) Wall-type structure; foil was uniaxially stretched before ablation ($\phi=60$ mJ/cm², $N_\ell=10$ laser pulses). (b) Nap-type structure; foil was biaxially stretched before ablation ($\phi=90$ mJ/cm², $N_\ell=10$ laser pulses). (c) Annealed foil ($\phi=90$ mJ/cm², $N_\ell=10$ laser pulses). After Refs. [7,1].

*On leave from Institute of Applied Physics, Russian Academy of Sciences, 603950, Nizhnii Novgorod, Russia.

†Corresponding author. Electronic address: dieter.baeuerle@jku.at

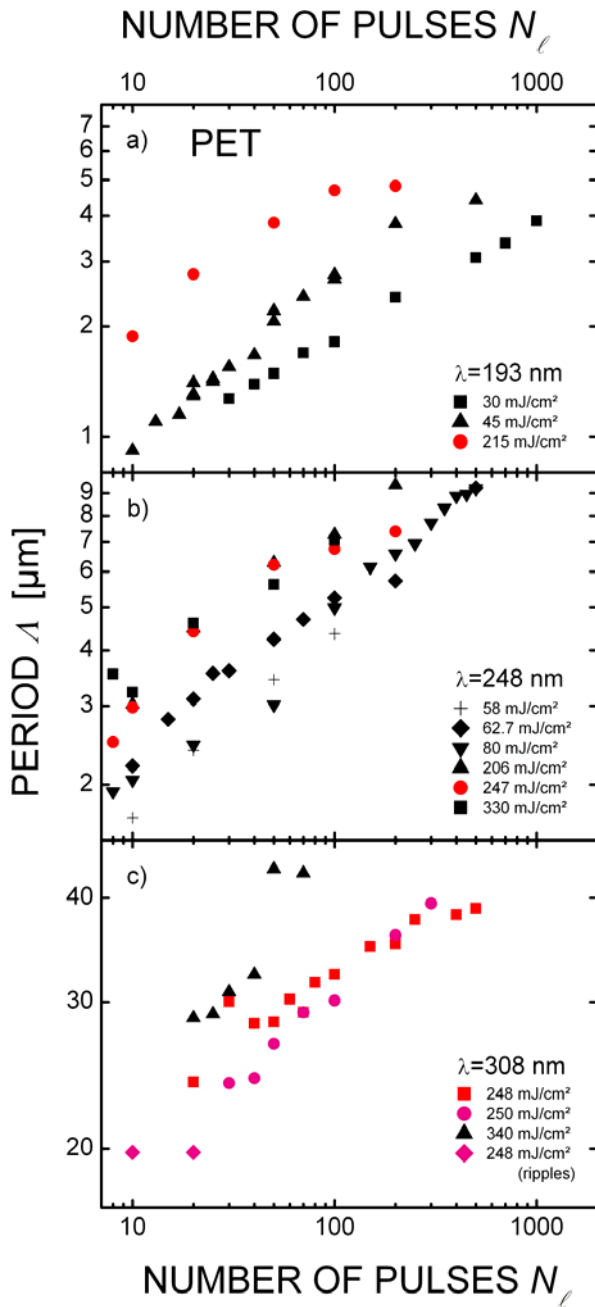


FIG. 2. (Color online) Period Λ of nap-type structures observed on biaxially stretched PET foils (Dupont MylarTM, thickness $50 \mu\text{m}$). Λ increases with the number of laser pulses N_ℓ , the laser wavelength, and fluence. (a) 193 nm ArF-, (b) 248 nm KrF-, and (c) 308 nm XeCl-excimer laser radiation.

observed upon full annealing [Fig. 1(c)]. Commercial polyimide foils (Upilex RTM and Kapton HTM) do or do not possess frozen-in stresses, depending on the particular fabrication process. In the latter case no noticeable structure formation was observed in the range of $N_\ell < 5000$ and laser fluences $20 \leq \phi \leq 330 \text{ mJ/cm}^2$ [6]. The dependence of the surface roughness on the number of laser pulses N_ℓ has been measured by atomic force microscopy (AFM). The results are shown in Fig. 4 for biaxially stretched PET foils irradiated with ArF and KrF laser light. As the original surface is plane

and the structures lead to quasiperiodic surface profile perturbations, the roughness R_a correlates with the depth of structures. As a rough estimate one can assume that the depth of structures a exceeds R_a at least twice.

III. THERMODYNAMICS OF PERIODIC PARALLEL INTERACTING CRACKS

A simple model for the formation of wall- and nap-type structures based on stress relaxation is presented in Ref. [1]. According to this model, frozen-in stresses within the polymer foil may relax under laser irradiation due to crack formation. The period of structures is determined by the minimum of the free energy. This, in turn, is determined by the decrease of the elastic energy and the increase in surface energy due to crack formation. Thus, the theoretically *optimum* period, Λ^* , will depend on the depth of cracks a , so that $\Lambda^* = \Lambda^*(a)$. Note, that we retain the notation Λ for the *experimentally* measured period.

Henceforth we assume that the stress is oriented along the x direction and that the cracks develop in the z direction (Fig. 5). The cracks shall be equidistant and of infinite length in the y direction. Using symmetry arguments we henceforth consider instead of this two-dimensional (2D) *semi-infinite* problem the interaction between parallel periodic cuts of length $2a$ in an *infinite* medium. As tangential stresses do not necessarily disappear in the symmetry plane, this problem only approximates the original one.

In the theory of fracture, the free energy of a crack is often described by a stress intensity factor K . It depends on the overall geometry of the crack and the specimen, as well as on the overall applied external stress. K characterizes the local behavior of the stress and strain near the tip and therefore the elastic energy in this region. The free energy *per unit length of a crack in the y direction*, Δf , increases with the depth a (note, that the cuts in an infinite medium have a length $2a$ and 2 tips). For uniform external tensile stress this increase can be described by the following equation from Ref. [10]:

$$\frac{\partial \Delta f}{\partial a} = 2\mu - \frac{(1 - \sigma_p^2)}{Y} K^2. \quad (1)$$

Here, Y is Young's modulus, σ_p is Poisson's ratio, and μ is the surface tension coefficient. The two terms refer to the surface and elastic energy, respectively. The coefficient $1 - \sigma_p^2$ is typical for 2D elastic problems [11]. A periodical set of cracks with spacing Λ within an infinite medium was studied in Refs. [10,12,13]. The shape of the opening satisfies an integral equation, which can be solved analytically if its kernel is approximated by a simpler function with correct asymptotics. The accuracy of this replacement is better than 10% everywhere. Using this approach, the stress intensity factor becomes [13]

$$K = \sigma_{xx} \sqrt{\frac{\Lambda \tanh(2\pi a/\Lambda)}{2}}. \quad (2)$$

The free energy per unit area of the film surface, ΔF , of the periodical array of cracks can now be obtained by integrating

TABLE I. Optical properties of PET at different wavelength and parameters used in the calculations.

Laser wavelength λ (nm)	193	248	308	
Ablation threshold ϕ_{th} (J/cm ²)	0.028	0.036	0.17	Refs. [18,25]
Fluence used for analysis $\phi \approx 1.5\phi_{th}$ (J/cm ²)	0.045	0.062	0.25	
Pulse duration τ (FWHM) (s)	15×10^{-9}	28×10^{-9}	30×10^{-9}	
Absorption coefficient α (cm ⁻¹)	3×10^5	1.6×10^5	4×10^3	Ref. [1]
Absorption length l_α (μ m)	0.033	0.063	2.5	
Thermal length $l_T \approx \sqrt{D_T \tau}$ (μ m) with $D_T = 10^{-3}$ (cm ² /s)	0.039	0.053	0.060	Ref. [1]
Thermal width at the end of the pulse $l_\alpha + l_T$ (μ m)	0.072	0.116	2.56	
Ratio $(l_\alpha + l_T) / \phi_{th}$	3.27	3.87	15.0	
Parameter N_0 (curve fitting in Fig. 7)	250	150	40	
Parameter Λ_∞ (curve fitting in Fig. 7) (μ m)	4.9	8.2	37	
Griffith length a_G [Eq. (15) and fitting data] (μ m)	1.17	2.03	1.87	

Eq. (1) with $K(a)$ from Eq. (2) and dividing the result by Λ . This yields

$$\Delta F = 2\mu \frac{a}{\Lambda} \left\{ 1 - \frac{\Lambda^2}{4\pi^2 a a_G} \ln \left[\cosh \left(\frac{2\pi a}{\Lambda} \right) \right] \right\}$$

$$\approx \begin{cases} 2\mu \frac{a}{\Lambda} \left(1 - \frac{a}{2a_G} \right) & \text{with } \Lambda \gg a \\ 2\mu \frac{a}{\Lambda} \left(1 - \frac{\Lambda a - \Lambda^2 (\ln 2/2\pi)}{2\pi a a_G} \right) & \text{with } \Lambda \ll a. \end{cases} \quad (3a)$$

$$(3b)$$

Here, we introduced the Griffith length

$$a_G = \frac{2\mu Y}{\pi(1 - \sigma_p^2)\sigma_{xx}^2}, \quad (4)$$

which is a well-known scale parameter in the theory of fracture and crack formation (see, e.g., Ref. [11]). The asymptotic behavior in Eqs. (3a) and (3b) can be easily understood by considering the limiting cases $\Lambda \gg a$ and $\Lambda \ll a$.

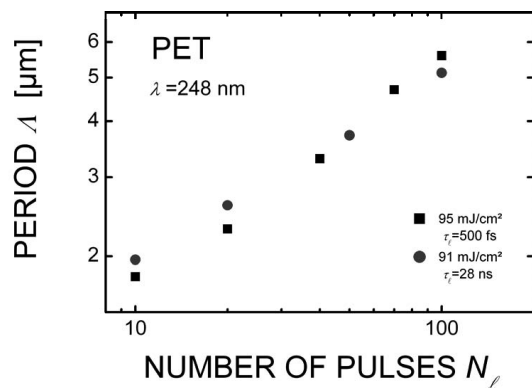


FIG. 3. Dependence of the period Λ of naps on the number of laser pulses N_ℓ for 500 fs and 28 ns KrF laser pulses ($\lambda=248$ nm).

A. Case $\Lambda \gg a$

This case describes noninteracting cracks. For isolated cracks the stress remains essentially unchanged except near the cracks (Saint-Venant's principle). The effective area of stress relaxation near a crack is $S \sim a^2$ [see Fig. 5(a)]. This immediately results in an expression similar to Eq. (3a). The crack propagates as long as $\partial\Delta F / \partial a < 0$. Thus, cracks will grow if

$$a > a_G. \quad (5)$$

This is the Griffith condition. It defines the minimum size of the seed crack for a given stress σ_{xx} . The situation is similar to nucleation theory where the growth of a particle or a thin film island requires a critical size of the nucleus. The stress necessary to generate a crack with the initial depth a , can be considered as having a "threshold" value. Material disintegration proceeds if

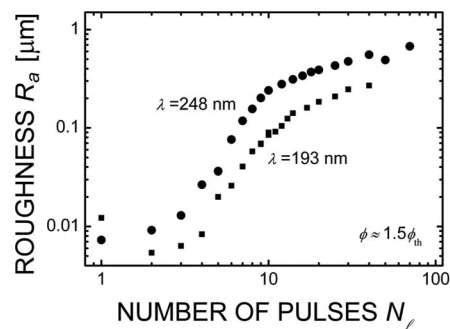


FIG. 4. Dependence of the average surface roughness R_a (root mean square deviation) of biaxially stretched PET foils on the number of laser pulses N_ℓ for 193 nm ArF (squares, 42 mJ/cm²) and 248 nm KrF laser radiation (circles, 58 mJ/cm²). The measurements have been performed by means of an AFM (10 μ m scan), contact mode. The laser fluences employed were $\phi \approx 1.5\phi_{th}$. The value of R_a correlates with (but is not equal to) the structure depth a , which cannot be measured directly. Note that the range of pulse numbers N_ℓ is different from that in Figs. 2 and 7.

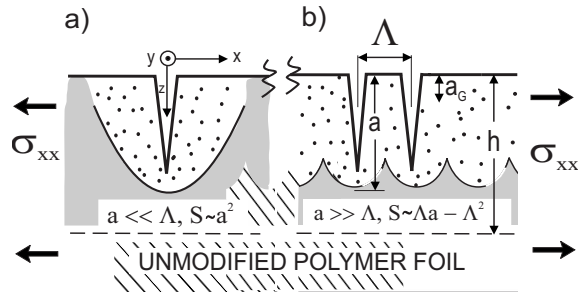


FIG. 5. Schematic picture of the limiting cases of stress relaxation. (a) Distant, noninteracting cracks with $\Lambda \gg a$. (b) Close, strongly interacting cracks with $\Lambda \ll a$. The dotted regions indicate the area S where the stress is relaxed.

$$\sigma_{xx} > \sqrt{\frac{2\mu Y}{\pi(1-\sigma_p^2)a}}. \quad (6)$$

With cracks of “overcritical” depth satisfying Eq. (5), the total free energy of the system will decrease with respect to its initial value if $\Delta F < 0$, i.e., for $a > 2a_G$. From Eq. (3a) we find that the overall decrease in energy is $\Delta F \propto -\Lambda^{-1}$. Thus, smaller periods are more favorable, as long as $\Lambda \gg a$. This condition does not hold if the depth of cracks grows. With numbers realistic for heated polymers $Y \approx 10^5$ N/cm², $\mu \approx 0.3 \times 10^{-5}$ J/cm², $\sigma_p \approx 0.25$, and frozen-in stresses $\sigma_{xx} \approx 3 \times 10^2$ N/cm² we obtain from Eq. (4) a Griffith length $a_G \approx 2.3$ μ m. These numbers deserve some discussion. The fracture of amorphous polymers is often described by the effective “fracture surface energy,” which for various polymers can be in the range $\mu \approx 10^{-2} - 2.5 \times 10^{-1}$ J/cm² and decreases with the temperature [14,15]. This is 3–4 orders of magnitude higher than the conventional coefficient of surface tension [14,15], which for PET at room temperature is about $\mu \approx 0.43 - 0.49 \times 10^{-5}$ J/cm² [16,17]. This is due to the contribution of plastic deformations near the tip of the crack and the formation of fibrils in this area (crazing) that also creates additional surfaces. We do not observe fibrils in the upper part of the crack, probably as they disappear upon ablation, but their existence near the tip cannot be excluded. In any case, higher effective values of μ still result in similar estimations for the Griffith length a_G if higher frozen-in stresses are assumed. Note that according to Eq. (6) a 100-fold increase in μ can be compensated by a 10-fold increase in σ_{xx} . The values of σ_{xx} of up to 10^4 N/cm² do not seem unrealistic assuming 10% shrinkage of PET upon heating and an elastic modulus of $Y \sim 10^5$ N/cm². This value of shrinkage was experimentally measured on commercial foils used in the experiments [18]. The values of Y depend strongly on the temperature, molecular weight, and degree of crystallinity of the PET, and lies within the range $10^3 < Y < 10^6$ N/cm² [19,20]. The manufacturer provides values of $Y \approx 3 \times 10^5$ N/cm² at room temperature and $Y \approx 1.5 \times 10^4$ N/cm² near the melting point [20]. As structure formation takes place at elevated temperatures, the value of 10^5 N/cm² seems suitable for our estimations.

B. Case $\Lambda \ll a$

In this case, the stress relaxes almost everywhere except within an area $\sim \Lambda^2$ near the bottom of cracks [see Fig. 5(b)].

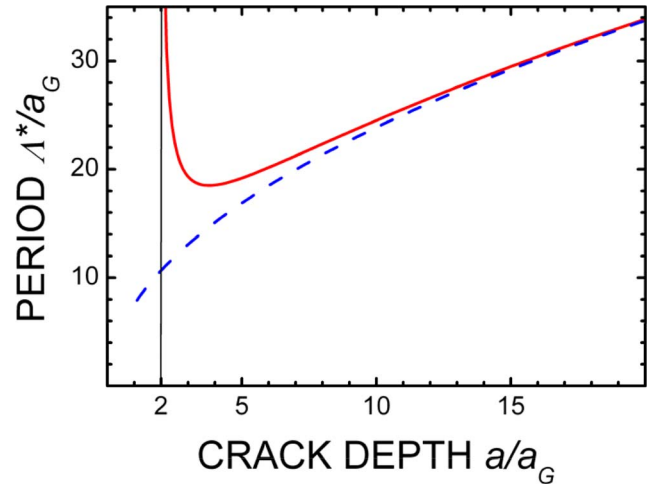


FIG. 6. (Color online) Dependence of the normalized optimal crack period Λ^*/a_G on the normalized depth a/a_G . Solid line, dependence (8). Dashed line, square root approximation (9). The optimum period is around $4a_G$.

The effective area of stress relaxation becomes $S \sim \Lambda a - \xi \Lambda^2$, where ξ is some dimensionless constant. This explains the origin of Eq. (3b), where the first term in brackets dominates. Thus, $\Delta F \propto a/\Lambda > 0$ decreases with Λ . Together with Eq. (3a), this means that ΔF has a minimum as a function of Λ .

This *optimum* spacing for a given a corresponds to this minimum of the free energy in Eq. (3). The condition for an extremum with respect to Λ can be written in a compact form as

$$\gamma_G = \tanh(\gamma) - \gamma^{-1} \ln(\cosh \gamma) \quad \text{with} \quad \gamma = \frac{2\pi a}{\Lambda}. \quad (7)$$

One can numerically solve this condition with respect to Λ and express the resulting *optimum* distance $\Lambda^*(a)$ in terms of universal dimensionless transcendental function Γ ,

$$\frac{\Lambda^*}{a_G} = \Gamma\left(\frac{a}{a_G}\right). \quad (8)$$

This dependence is shown in Fig. 6. With $a > 2a_G$ the overall energy decreases with the growth of cracks. As the depth a increases, Λ^* drops first very sharply, reaches a minimum at $a \approx 4a_G$, and then increases again. In the limit $a \gg a_G$, which entails $a \gg \Lambda$, differentiating the second asymptotic (3a) yields

$$\Lambda^* = \frac{2\pi}{\sqrt{\ln 2}} \sqrt{a_G a} \propto \sigma_{xx}^{-1}. \quad (9)$$

The fact that the energy minimum can be obtained from the asymptotic expression (3b) reveals that for *deep cracks* this minimum originates from the interaction between *closely spaced cracks* with $a \gg \Lambda \gg a_G$. The inverse proportionality of Λ^* to the frozen-in stress in Eq. (9) is difficult to verify experimentally, as for small stresses the Griffith length (4) becomes very large. This suppresses or even prevents structure formation.

Figure 6 demonstrates that Eq. (9) is a good approximation for $a/a_G \geq 10$. In this region the free energy estimated from Eq. (3b) is

$$\Delta F(\Lambda^*) \approx 2\mu \left(\frac{\sqrt{\ln 2}}{2\pi} \sqrt{\frac{a}{a_G}} - \frac{a}{2\pi a_G} \right). \quad (10)$$

This shows that for cracks with $a \geq a_G$ the free energy at the optimum spacing decreases with increasing a . Thus, cracks will continue to deepen. With increasing a , the energetically favored period $\Lambda^*(a)$ will increase as well. This may take place via merging of neighboring cracks. Too frequent cracks are suppressed by the surface tension. The development of structures ceases when the depth of cracks approaches the thickness of the modified layer h . Alternatively, kinetic restrictions may suppress this process.

The transformation from a semi-infinite space to the full space problem is justified, as long as the middle and the tip of the cracks do not influence each other. This requires $a \gg \Lambda^*$ because differences due to free boundary in the semi-infinite-space problem will be localized over the area $\sim \Lambda^{*2}$ near the surface. Therefore, the square root dependence (9) justifies the full space approximation as long as $a \gg a_G$.

More rigorous solutions for the problem of parallel interacting cracks [21,22] that calculate asymptotic expressions for the width of cracks and the stress intensity factor without the approximations used in Ref. [13] produce similar results.

Up to now we considered structure formation based on *uniaxial* stresses only. However, in the lowest order, the theoretical considerations can be applied to biaxially stretched materials as well. In the conventional theory, in the absence of tensile frozen-in stresses, crack formation is not influenced by the stress component parallel to the groove [13]. This means that in the first approximation cracks in perpendicular directions can be treated independently.

IV. COMPARISON WITH EXPERIMENTAL DATA

The preceding model permits one to describe the most characteristic features of wall- and nap-type structures formed during laser ablation of uniaxially and biaxially stretched polymer foils. In particular, the optimal period of structures Λ , the depth of structures or cracks a , and the thickness of the modified layer h are interrelated. According to Eq. (9), the optimal period Λ^* is proportional to \sqrt{a} . Figures 2, 3, and 7 show that pronounced structures are usually observed with $N_\ell > 10$ pulses only. In such multiple-pulse experiments, the depth of structures or cracks a , may increase due to the increasing thickness of the modified layer h . According to our assumptions, cracks can propagate only within the modified layer. Thus, the dependence $\Lambda^*(N_\ell)$ is related to the increase in h with the number of laser pulses, i.e., $h=h(N_\ell)$.

The real situation may be, however, more complicated. The saturation in the depth of the modified layer may be augmented by kinetic limitations as well. It is well known that relaxation processes in polymers are temperature dependent. Thus, a certain threshold temperature is needed for the growth of cracks. This temperature can be rather low. For

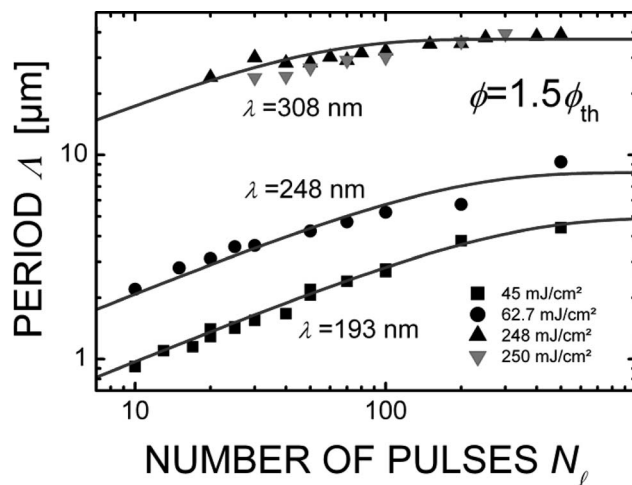


FIG. 7. Fit of experimental data $\Lambda = \Lambda(\lambda, N_\ell)$ by means of Eq. (13) for the optimum spacing Λ^* . The parameters employed are listed in Table I.

example, it may be related to the glass temperature (for PET $T_G \approx 70^\circ\text{C}$, $\Delta T_G \approx 50\text{K}$) or to the softening of material near the melting point (for PET $T_G \approx 260^\circ\text{C}$, $\Delta T_G \approx 240\text{K}$). In this case the depth of cracks will saturate at some limiting value a_∞ , as the necessary temperature is never achieved beyond this depth. The physical nature of modification is most probably related to amorphization. One cannot exclude additional, possibly inhomogeneous, photochemical changes or chemical modifications such as oxygen diffusion and carbonization, but these are more fine effects that may modify material and process parameters, but do not alter the overall picture of the effect.

Estimations show, however, that for both thermal and photochemical models, the thickness of the modified layer either saturates within 2–10 pulses, or grows only logarithmically, i.e., much slower than the typical saturation observed in the period and depth of the structures (Figs. 2 and 3). Because it is difficult to unambiguously establish whether modified depth or kinetic effects are responsible for the saturation in the depth of structures, we assume that with multiple pulse experiments both mechanisms result in comparable limiting depths $h_\infty \sim a_\infty$. Thus, we adopt the simplest possible form of relaxation,

$$\frac{da}{dN_\ell} = \frac{a_\infty - a}{N_0}, \quad (11)$$

where a_∞ and N_0 are parameters describing saturated depth and the number of pulses required to approach it. The solution of this equation yields

$$a = a_\infty \{1 - \exp(-N_\ell/N_0)\}. \quad (12)$$

If the cracks are not in thermodynamic equilibrium, their spacing depends on the detailed 3D kinetics of growth that is difficult to assess. If however, the (lateral) growth is fast enough, the energetically optimal relationship (9) between the crack depth a and period Λ^* is maintained throughout the growth process. This results in

$$\Lambda^* = \Lambda_\infty \sqrt{1 - \exp(-N_\ell/N_0)} \quad \text{with} \quad \Lambda_\infty = \frac{2\pi}{\sqrt{\ln 2}} \sqrt{a_G a_\infty}. \quad (13)$$

Equation (13) was used for fitting the experimental results in Fig. 7. Its validity is justified retrospectively by the subsequent analysis. The fitting parameters are listed in Table I. For the sake of generality, we do not bound the parameters for N_0 and a_∞ (which defines Λ_∞) to any particular microscopic model. Instead, we discuss their physically admissible range within the framework, which holds for the broad variety of thermal models.

Near the ablation threshold at the end of the laser pulse, the absorbed fluence is about equal to the heat content within the material: $\phi_a \sim \Delta T_v c \rho (l_\alpha + l_T)$, where l_T is the thermal length for the duration of the laser pulse and $\Delta T_v \sim 800\text{--}900$ K is the characteristic temperature of ablation (referred to as room temperature), which is about the same for all wavelengths [1,23]. If the temperature needed for material modification and/or the growth of cracks is denoted as T_G , the energy conservation between the end of the laser pulse and the farthest advance of T_G isotherm can be written as $\Delta T_v c \rho (l_\alpha + l_T) \sim \Delta T_G c \rho a_\infty$, which results in

$$a_\infty \sim \frac{\Delta T_v}{\Delta T_G} (l_\alpha + l_T). \quad (14)$$

This means that a_∞ is several times larger than the heat affected zone at the end of the laser pulse. At employed fluences, that are only moderately above the ablation threshold, typical ablation rates are of the order of 40–100 nm/pulse (the last value is for 308 nm) [18]. This is much less than the depth of observed structures and the estimated thickness of the modified layer, which lie in the several microns range. For this reason, henceforth we neglect the influence of ablation on structure formation, though it may play a role, especially for the development of initial cracks.

A distinctive robust feature of the fitting performed in Fig. 7 is a square root dependence of the optimal period Λ^* on the number of pulses in the unsaturated stage $N_\ell \ll N_0$, which reflects the square root dependences in Eqs. (9) and (13). This dependence is also confirmed by estimations of the Griffith length from the fitting parameters using relations (13) and (14),

$$a_G \approx \frac{\Lambda_\infty^2}{(2\pi)^2 \frac{\Delta T_v}{\Delta T_G} (l_\alpha + l_T)}. \quad (15)$$

As ΔT_G is limited from above by the melting temperature (~ 260 °C for PET [18–20]), $\Delta T_v/\Delta T_G \sim 5$ is used in further estimations. This yields a value of a_G , which is in the micron range for all wavelengths employed (see Table I). These values are also consistent with theoretical estimations based on Eq. (4). The result is not very sensitive to the details of the underlying mechanisms, as Λ_∞ is an experimentally deduced fitting parameter. The heat affected zone $l_\alpha + l_T$ can be reliably estimated, and the ratio $\Delta T_v/\Delta T_G$ cannot deviate from the assumed value by more than a factor of 2. The robustness

of the result justifies the framework of our considerations.

The saturation number of pulses N_0 can be estimated in the following way. From Eq. (11) with $a \sim 0$ one can see that the ratio a_∞/N_0 gives the increment in the structure depth per pulse Δa in the initial unsaturated regime. The order of magnitude of this quantity is $\Delta a \sim kt$, where k is the typical rate of growth of cracks and t is the time during which the material remains heated after a single pulse. It is determined by the thermal time, $t \propto (l_\alpha + l_T)^2/D_T$, where D_T is the thermal diffusivity of the material. For comparable experimental conditions ($\phi/\phi_{th} \approx 1.5$) the temperature and therefore the growth rates k are similar for all laser wavelengths. Thus, we can write $\Delta a \sim a_\infty/N_0 \propto kt_G \propto k(l_\alpha + l_T)^2/D_T$, and substituting a_∞ from Eq. (14) one obtains the estimation for N_0 (dimensionless prefactors omitted),

$$N_0 \propto D_T/k(l_\alpha + l_T). \quad (16)$$

This equation implies that $(l_\alpha + l_T)N_0 \sim \text{const}(\lambda)$, which correlates with the fitting results apart from the data at 308 nm.

A. Influence of absorption coefficient

Equations (13) and (14) suggest a square root dependence of the optimal period Λ^* on the thermal length, which for large wavelength (e.g., 308 nm) is dominated by the absorption length. It is confirmed by Figs. 2 and 7 as well as by the parameters and results listed in Table I. Note that the effective absorption coefficients reported in the literature on laser ablation vary somewhat, [1,24], especially at high fluences (up to 2 J/cm² for XeCl [25]). The same is true for ablation thresholds, probably due to differences in laser pulse duration. The fluences used in the experiments with 248 nm KrF laser radiation were somewhat higher than $1.5\phi_{th}$. Especially for 308 nm in the multiple-pulse regime, incubation effects become important [18]. These increase the effective absorption coefficient.

B. Laser fluence

Above the ablation threshold, T_v increases logarithmically with the fluence [1], and so should the depth and the spacing of cracks, as suggested by Eqs. (13) and (14). With multiple pulses, the situation is qualitatively similar, i.e., a sublinear dependence $\Lambda(\phi)$ is expected. This is in qualitative agreement with Fig. 2—the period of structures increases only moderately with laser fluence and almost saturates at $\phi \approx 2\text{--}4\phi_{th}$ [Fig. 2(b)].

C. Pulse length

Within the accuracy of measurements, there is no difference in $\Lambda = \Lambda(N_\ell)$ dependence between fs and ns irradiation, at least with the laser fluences employed in the experiments, $\phi \sim 95$ mJ/cm² (Fig. 3). We can tentatively explain this observation in the following way. Ablation rates are similar for ns and fs pulses for fluences below 100 mJ/cm² and are around 60–80 nm/pulse for 248 nm at these fluences [18,26]. In both cases most of the crack formation takes place *after* the pulse, when the ablation has stopped already. The depth of the heat affected zone should certainly increase

for ns irradiation due to heat diffusion (see Table I). On the other hand, with fs pulses and strongly absorbing materials such as PET at 248 nm, bleaching effects may become important. These may compensate the decrease in heat penetration depth. This is supported by a simple estimation: the short-pulse saturation condition is $\sigma\phi/\hbar\omega \geq 1$ where σ is the absorption cross section per electronic transition and $\hbar\omega = 8 \times 10^{-19}$ J. For PET one can estimate σ (248 nm) $\sim 3.5 \times 10^{-17}$ cm² assuming one chromophore per monomer unit. For PET the chromophore group that provides the strong absorption cross section at 248 nm is most probably a benzene ring surrounded by two C=O groups. Therefore, the onset of saturation is expected at laser fluences $\phi \sim 30$ mJ/cm², well below the fluences employed (Fig. 3). At lower fluences bleaching should be less pronounced. Indeed, preliminary experiments with $\phi \sim 50$ mJ/cm² reveal that the period observed with fs laser irradiation and $N_\ell = 10$ is noticeably smaller than for ns pulses. This supports the argumentation that the heat affected zone is larger with ns pulses if bleaching is absent.

V. CONCLUSIONS

Wall- and nap-type structures observed in laser ablation of stretched polymer foils can be interpreted on the basis of an optimally spaced system of cracks that develop within the modified surface layer. The model satisfactorily explains the dependence of the spacing of structures on the number of laser pulses, the absorption coefficient at the laser wavelength employed, and on the laser fluence.

The minimization of the free energy reveals the following features: Cracks of a given depth a grow if a certain thresh-

old value of the stress is exceeded. Alternatively, for a given stress, the corrugation will grow if it exceeds a threshold depth a_G (Griffith). If initial cracks are deep enough, $a \geq 4a_G$, the energetically optimal period of the pattern Λ^* follows a square root dependence $\Lambda^* \approx 7.5\sqrt{a_G a}$.

The dependence of the period of patterns on laser fluence and the number of laser pulses can be attributed to two factors—the dependence of the thickness of the modified layer h on these parameters, and the kinetics of the growth of cracks. It is difficult to unambiguously discriminate between them, but for both mechanisms the depth of cracks correlates strongly with the thickness of the heat affected zone during the pulse.

The comparison of the theoretical results and the experimental data obtained for PET at excimer laser wavelengths of 193, 248, and 308 nm, shows a qualitative agreement. The period of structures first increases with the square root of the number of pulses N_ℓ and becomes almost independent of N_ℓ with $N_\ell \geq 200$ pulses. There exists a strong correlation between the absorption length and the period Λ .

Due to ablation the thickness of the modified layer changes only slightly with laser fluence [1]. Additionally, material ablation may be crucial in the development of the initial roughness and the creation of supercritical crack nuclei, for example, due to instabilities of the plain ablation front. A detailed consideration of all of these mechanisms is beyond the scope of this paper.

ACKNOWLEDGMENT

One of us (D.B.) gratefully acknowledges financial support by the Austrian Research FWF (Fonds zur Förderung der wissenschaftlichen Forschung) under Contract No. P16133–N08.

-
- [1] D. Bäuerle, *Laser Processing and Chemistry*, 3rd ed. (Springer, Berlin, 2000).
 - [2] T. Bahnert and E. Schollmeyer, *Angew. Makromol. Chem.* **151**, 39 (1987).
 - [3] T. Bahnert and E. Schollmeyer, *J. Appl. Phys.* **66**, 1884 (1989).
 - [4] E. Arenholz, J. Heitz, V. Svorcik, and D. Bäuerle, in *Excimer Lasers*, edited by L. D. Laude, NATO Advanced Studies Institute Series E: Applied Sciences (Kluwer Academic, Dordrecht, 1994), Vol. 265, p. 237.
 - [5] E. Arenholz, J. Heitz, M. Wagner, D. Bäuerle, H. Hibst, and A. Hagemeyer, *Appl. Surf. Sci.* **69**, 16 (1993).
 - [6] E. Arenholz, M. Wagner, J. Heitz, and D. Bäuerle, *Appl. Phys. A: Solids Surf.* **55**, 119 (1992).
 - [7] E. Arenholz, V. Svorcik, T. Kefer, J. Heitz, and D. Bäuerle, *Appl. Phys. A: Solids Surf.* **53**, 330 (1991).
 - [8] Y. Novis, J. J. Pireaux, A. Brezini, E. Petit, R. Caudano, P. Lutgen, G. Feyder, and S. Lazare, *J. Appl. Phys.* **64**, 365 (1988).
 - [9] V. I. Emel'yanov and K. I. Eriomin, *Proc. SPIE* **3343**, 1056 (1998).
 - [10] L. I. Slepyan, *Mehanika Treschin (Mechanics of Cracks)* (Sudostroenie, Leningrad, 1981) (in Russian).
 - [11] L. D. Landau and E. M. Lifshitz, *Theory of Elasticity*, 3rd ed. (Pergamon, Oxford, 1986).
 - [12] N. I. Muskhelishvili, *Some Basic Problems of the Mathematical Theory of Elasticity* (Noordhoff International, Leyden, 1977).
 - [13] V. V. Panasyuk, M. P. Savruk, and A. P. Dashyzyn, *Raspreделение Napryazhenii Okolo Treschin v Platinah i Obolochkah (Distribution of Stresses Near the Cracks in Plates and Shells)* (Naukova dumka, Kiev, 1976) (in Russian).
 - [14] G. Strobl, *The Physics of Polymers*, 3rd ed. (Springer, Berlin, 1997).
 - [15] J. P. Berry, *Fracture of Polymeric Glasses* (Academic, New York, 1972), Chap. 2.
 - [16] H. G. Elias, *Makromoleküle, Band 2—Physikalische Strukturen Und Eigenschaften*, 6 Aufl. (Wiley-VCH, Weinheim, 2001).
 - [17] <http://www.igb.fraunhofer.de/www/gf/GrenzflMem/gf-physik/en/GFphys-PolymOberfl.en.html>
 - [18] E. Arenholz, Ph.D. thesis, Johannes-Kepler-University, Linz, 1994 (unpublished).
 - [19] A. J. Peacock, *Handbook of Polyethylene* (Dekker, New York, 2000).

- [20] <http://www.dupontteijinfilms.com/datasheets/mylar/productinfo/properties/h37232-3.pdf>
- [21] B. I. Smetanin, *Inzh. Zh., Mekh. Tverd. Tela* **3**, 115 (1968) (in Russian) [*Mech. Solids* **3**, 112 (1968)].
- [22] M. Alexandrov and B. I. Smetanin, *Prikl. Mekh.* **29**, 782 (1965) (in Russian) [*J. Appl. Math. Mech.* **29**, 926 (1965)].
- [23] N. Arnold, B. Luk'yanchuk, and N. Bityurin, *Appl. Surf. Sci.* **127**, 184 (1998).
- [24] S. Petit, P. Laurens, J. Amouroux, and F. Arefi-Khonsari, *Appl. Surf. Sci.* **168**, 300 (2000).
- [25] J. E. Andrew, P. E. Dyer, D. Forster, and P. H. Key, *Appl. Phys. Lett.* **43**, 717 (1983).
- [26] J. Heitz, E. Arenholz, D. Bäuerle, R. Sauerbrey, and H. M. Phillips, *Appl. Phys. A: Solids Surf.* **59**, 289 (1994).